annalen der physik

www.ann-phys.org

Unveiling the Link Between Fractional Schrödinger Equation and Light Propagation in Honeycomb Lattice

Da Zhang, Yiqi Zhang, Zhaoyang Zhang, Noor Ahmed, Yanpeng Zhang, Fuli Li, Milivoj R. Belić, and Min Xiao*

We suggest a real physical system — the honeycomb lattice — as a possible realization of the fractional Schrödinger equation (FSE) system, through utilization of the Dirac-Weyl equation (DWE). The fractional Laplacian in FSE causes modulation of the dispersion relation of the system, which becomes linear in the limiting case. In the honeycomb lattice, the dispersion relation is already linear around the Dirac point, suggesting a possible connection with the FSE, since both models can be reduced to the one described by the DWE. Thus, we propagate Gaussian beams in three ways: according to FSE, honeycomb lattice around the Dirac point, and DWE, to discover universal behavior — the conical diffraction. However, if an additional potential is brought into the system, the similarity in behavior is broken, because the added potential serves as a perturbation that breaks the translational periodicity of honeycomb lattice and destroys Dirac cones in the dispersion relation.

1. Introduction

The fractional Schrödinger equation (FSE) is the fundamental equation of the fractional quantum mechanics.[1–3] As compared to the standard Schrödinger equation, it contains the fractional Laplacian operator instead of the usual one. This change brings profound differences in the behavior of wave function. In optics, the fractional Laplacian corresponds to a non-parabolic dispersion, which means that the dispersion of the system is directly modulated. Interesting phenomena based on the FSE were reported in the past few years[4–7] and some related nonlinear aspects were discussed.[8–11] The complicated fractional Laplacian operation in the FSE is made more manageable if one uses the Fourier transform method in both theory and experiment;[12] however, the real problem is the lack of real physical systems described directly by the FSE. Here, one of our aims is to point at such a system. The other aim is to describe this system from different points of view.

The topological photonics[13] — as a new field — has experienced an explosive development and still attracts great attention. Among different photonic models that are explored, the honeycomb lattice (viz. the photonic graphene)[14,15] has excited particular interest. Research on honeycomb lattice has inspired new ideas to develop new techniques and methods in optical manipulation, image transmission, and optical trapping, to name a few. The goal of this paper is to investigate whether the honeycomb lattice can be used as a real physical system described by FSE, which usually is not related to the description by the standard Schrödinger equation. The inspiration for this investigation comes from the fact that conical diffraction can be observed in both the evolution described by the FSE and in the evolution described by the Schrödinger equation in honeycomb lattice. Therefore, one has reasons to believe that the cause behind might be similar in the two systems. Indeed, the dispersion around the Dirac point in honeycomb lattice is nearly linear,[16] which indicates that the dispersion is effectively modulated — a consequence that can also arise in FSE, due to the fractional Laplacian. However, the connection is not straightforward.

Hence, in this paper we first demonstrate the transformation of the FSE into a Dirac-Weyl-like equation, and then the construction of the corresponding honeycomb lattice by using the three-wave interference method of light propagation. The band structure is calculated by the plane-wave expansion method. Then, we numerically simulate light evolution described by FSE, DWE, and the honeycomb lattice based on the usual Schrödinger equation, and note apparent similarities that point to similar origins. Two typical cases — direct and oblique excitation of the Bloch modes of the Dirac cone — are discussed in some detail. Finally, we give

D. Zhang, Y. Q. Zhang, Z. Y. Zhang, N. Ahmed, Y. P. Zhang
Key Laboratory for Physical Electronics and Devices of the Ministry of Education & Shaanxi Key Lab of Information Photonic Technique, Xi'an Jiaotong University
Xi'an, 710049, China
E-mail: zhangyiqi@mail.xjtu.edu.cn
Y. Q. Zhang, Z. Y. Zhang, F. L. Li
Department of Applied Physics
School of Science, Xi'an Jiaotong University
Xi'an, 710049, China
M. R. Belić
Science Program, Texas A & M University at Qatar
P.O. Box 23874, Doha, Qatar
M. Xiao
Department of Physics
University of Arkansas
Fayetteville, Arkansas, 72701, USA
National Laboratory of Solid State Microstructures and School of Physics, Nanjing University
Nanjing, 210093, China

DOI: 10.1002/andp.201700149

a discussion on the breakup of the model when harmonic potential is added, leading to the translational symmetry breaking and the disappearance of the Dirac point in the band structure. We believe that our research may pave way in the exploration of real physical systems that can be described by the FSE directly. It is also worth mentioning that such an attempt can be extended to networks, polariton condensates, as well as to the description of the Lévy transport in slab geometry of inhomogeneous media.

The organization of the paper is as follows. In Sec. 2, we first demonstrate the reduction of the FSE to the Dirac-Weyl-like equation, and then through the construction of the honeycomb lattice by the three-wave interference method, connect the same again with the DWE. The corresponding band structure is investigated by the plane-wave expansion method. In Sec. 3, we numerically simulate the light propagation in the three models: the FSE, the DWE, and the honeycomb lattice. The typical cases of directly and obliquely exciting the Bloch mode of the Dirac cone are discussed in Subsecs. 3.1 and 3.2. We conclude the paper in Sec. 4. We believe that our research may pave way to the exploration of other real physical systems that can be described by the FSE.

2. Theoretical Modeling

Some preliminaries from the fractional calculus are in order. We start with the two-dimensional FSE without potential[4–6]

$$i\frac{\partial\psi}{\partial z}-\left(-\frac{\partial^2}{\partial x^2}-\frac{\partial^2}{\partial y^2}\right)^{\alpha/2}\psi=0, \tag{1}$$

for the slowly-varying envelope ψ of the optical field. Here, z is the normalized propagation distance, and x and y are the scaled transverse coordinates; finally, α is the Lévy index ($1<\alpha\leq 2$). When $\alpha=2$, one recovers the usual Schrödinger equation in free space. We will consider here the opposite limiting case $\alpha=1$, as the most interesting.[12] The z-component of the generalized fractional angular momentum operator of order ζ can be written as

$$\hat{L}_z^{\zeta}=i\left(x\partial_y^{\zeta}-y\partial_x^{\zeta}\right).$$

Considering its commutation relation with the Hamiltonian $\hat{H}^{\alpha}=\sqrt{-\partial_x^2-\partial_y^2}$ of the FSE,

$$\left[\hat{L}_z^{\zeta},\,\hat{H}^{\alpha}\right]=-\alpha\left(\partial_x^{\alpha-1}\partial_y^{\zeta}-\partial_x^{\zeta}\partial_y^{\alpha-1}\right)\neq 0,$$

one infers that there should be an additional contribution, coming from the spin or intrinsic angular momentum.[17] So, one assumes that the field envelope $|\psi\rangle$ can be written as a multicomponent field

$$|\psi\rangle=(\psi_1,\ldots\psi_N)^T.$$

Namely, if one writes the usual Laplacian operator as

$$\hat{\mathcal{L}}=-\left(\frac{\partial^2}{\partial x^2}+\frac{\partial^2}{\partial y^2}\right), \tag{2}$$

one can factorize it as $\hat{\mathcal{L}}=\hat{\mathcal{L}}_+\hat{\mathcal{L}}_-$, where $\hat{\mathcal{L}}_+=\partial_x+i\partial_y$,$\hat{\mathcal{L}}_-=-\partial_x+i\partial_y$. Similarly, one can multiply both sides of Eq. (1) with the fractional Hamiltonian, to obtain:

$$\begin{aligned}\hat{H}^{\alpha}\hat{H}^{\alpha}|\psi\rangle&=\hat{\mathcal{L}}|\psi\rangle=\hat{\mathcal{L}}_+\hat{\mathcal{L}}_-|\psi\rangle\\&=\left(\hat{\mathcal{L}}_+\hat{\beta}^{\dagger}\right)\left(\hat{\beta}\hat{\mathcal{L}}_-\right)|\psi\rangle=E\,E|\psi\rangle,\end{aligned} \tag{3}$$

where $\hat{\beta}$ is $N\times N$ Hermitian matrix introduced to ensure the conservation of probability. Taking into account the uniformity of time and space, $\hat{\beta}$ should be independent of $(\hat{r},t)$ – that is, a constant matrix. Multiplying Eq. (3) with $\langle\psi|$ from the left and utilizing the completeness condition leads to

$$\langle\psi|\left(\hat{\mathcal{L}}_+\hat{\beta}^{\dagger}\right)|\psi\rangle\langle\psi|\left(\hat{\beta}\hat{\mathcal{L}}_-\right)|\psi\rangle=\langle\psi|E|\psi\rangle\langle\psi|E|\psi\rangle,$$

which can be rewritten as

$$\frac{\langle\psi|E|\psi\rangle}{\langle\psi|\left(\hat{\mathcal{L}}_+\hat{\beta}^{\dagger}\right)|\psi\rangle}=\frac{\langle\psi|\left(\hat{\beta}\hat{\mathcal{L}}_-\right)|\psi\rangle}{\langle\psi|E|\psi\rangle}. \tag{4}$$

It is reasonable to assume that both sides of Eq. (4) can be made equal to a non-zero constant s. Therefore, one obtains

$$i\frac{\partial\psi}{\partial z}-s\hat{\beta}\hat{\mathcal{L}}_+\psi=0,\qquad i\frac{\partial\psi}{\partial z}-\frac{1}{s}\hat{\beta}\hat{\mathcal{L}}_-\psi=0,$$

as an equivalent system of equations to Eq. (1).

Any single component (ψ_i) of the wave function ψ should satisfy the D'Alembert equation. We conclude that $\hat{\beta}$ must meet the anti-commutation relation $\hat{\beta}_i\hat{\beta}_j+\hat{\beta}_j\hat{\beta}_i=\delta_{ij}$, with $i,j=x,y,z$. Combining these properties of Hermitian matrices, anti-commutation relations, and $\hat{\beta}^2=1$, it becomes clear that in the case $N=2$ the Pauli matrices will appear. In the following, we use the Pauli operator σ_x to replace $\hat{\beta}$. On the other hand, the above coupled equations must satisfy the local probability conservation condition, which demands $s=1/s=1$. The speed of the spread of the two components should be the same, which also leads to $|\mathbf{k}|/s=s|\mathbf{k}|\Rightarrow s=1$. As a result, one ends up with

$$i\frac{\partial}{\partial z}\psi=\begin{bmatrix}0&\mathcal{L}_+\\\mathcal{L}_-&0\end{bmatrix}\psi\quad\text{or}\quad i\frac{\partial}{\partial z}\psi=\begin{bmatrix}0&\mathcal{L}_-\\\mathcal{L}_+&0\end{bmatrix}\psi. \tag{5}$$

Clearly, Eq. (5) is a Dirac-Weyl-like equation, which describes the spin-1/2 fermions. Without loss of generality, we use the first equation.

It is interesting to note that the DWE can be obtained from the usual Schrödinger equation with a potential described by the honeycomb lattice at the Dirac points.[18–21] The propagation of light in such a honeycomb lattice can be described by the usual Schrödinger equation[18,22]

$$i\frac{\partial\psi}{\partial z}+\nabla^2\psi+V_h(x,y)\psi=0, \tag{6}$$

in which the Laplacian is $\nabla^2=\partial_x^2+\partial_y^2$ and $V_h(x,y)$ is a periodic potential that can be connected with the intensity pattern of the three interfering plane waves. In other words, the missing link between Eqs. (1) and (6) is the DWE (5); i.e., the propagation dynamics according to the FSE with $\alpha=1$ can be mimicked by the

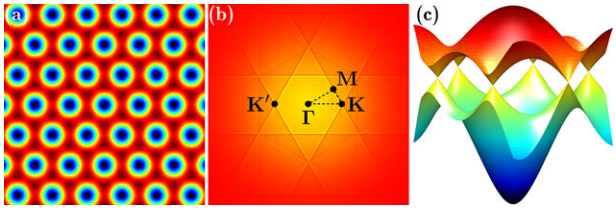

Figure 1. (a) Honeycomb lattice resulting from the three-wave interference with $k_0 = 1$. (b) Brillouin zone spectroscopy due to the far-field diffraction pattern, in which the high-symmetry points **Γ**, **M**, **K** and **K**′ of the first Brillouin zone are displayed. (c) The corresponding band structure with $V_0 = 1$.

Schrödinger equation around Dirac points in the honeycomb lattice. The deduction of DWE around a Dirac point from Eq. (6) is presented in Appendix; one may also consult other literature.[18,19]

The periodic potential that results from the intensity pattern of the three interfering plane waves[23] can be written as

$$V_h(x, y) = V_0 \left(9 - \left| \sum_{j=1}^{3} \exp\left(i k_0 \mathbf{b}_j \cdot \mathbf{r} \right) \right|^2 \right), \tag{7}$$

where V_0 indicates the input beam intensity, k_0 is used to scale the lattice constant, and $\mathbf{b}_1 = (1, 0)$, $\mathbf{b}_2 = (-1/2, \sqrt{3}/2)$, and $\mathbf{b}_3 = (-1/2, -\sqrt{3}/2)$ are the three unit vectors used to build the lattice. The honeycomb lattice obtained from Eq. (7) is displayed in **Figure 1**(a). One calculates the lattice constant — the distance between the two sites — as $4\pi/(3\sqrt{3}k_0)$. According to the far-field diffraction patterns,[24–27] one can obtain the corresponding Brillouin zone spectroscopy of the honeycomb lattice as shown in Fig. 1(b), in which the high symmetry points of interest, $\mathbf{\Gamma}(0, 0)$, $\mathbf{M}(3k_0/4, \sqrt{3}k_0/4)$, $\mathbf{K}(k_0, 0)$ and $\mathbf{K}'(-k_0, 0)$ are separately labeled.

For the construction of the corresponding band structure, we adopt the plane-wave expansion method.[6,18,28,29] The solution of Eq. (6) can be written as $\phi_n(\mathbf{r}; \mathbf{k}) \exp[i\beta_n(\mathbf{k})z]$, in which $\phi_n(\mathbf{r}; \mathbf{k})$ is the Bloch mode and $\beta_n(\mathbf{k})$ is the corresponding propagation constant. Plugging this solution into Eq. (6), one obtains

$$-\beta_n \phi_n + \nabla^2 \phi_n + V_h(x, y)\phi_n = 0, \tag{8}$$

which is the standard eigenvalue problem in band calculations. The calculated band structure is displayed in Fig. 1(c). As expected, there are six Dirac cones at the high-symmetry points **K** and **K**′ in the first Brillouin zone.

3. Numerical Simulations

In the following, we numerically demonstrate that light propagation in the FSE with $\alpha = 1$ can be well mimicked by the propagation in the honeycomb lattice. In addition, the inadequacy of such mimicking is also discussed, once an additional potential is included. We first consider and compare the propagation of Gaussian beams in the FSE, DWE, and honeycomb lattice. This is displayed in **Figure 2**.

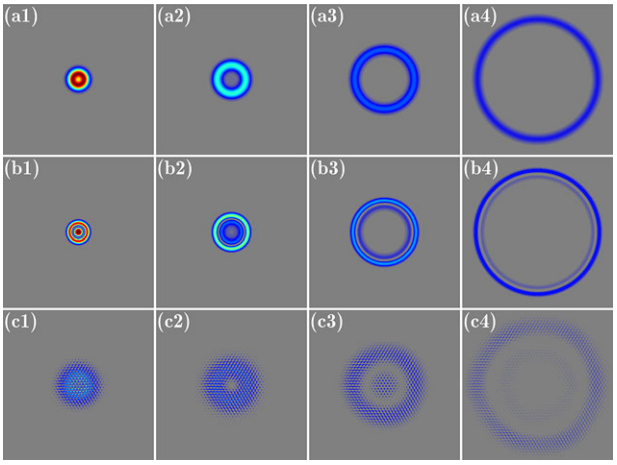

Figure 2. (a1)-(a4) Intensity distribution of light propagating according to FSE at $z = 10$, 20, 40 and 80. (b1)-(b4) Same as (a1)-(a4), but according to DWE. (c1)-(c4) Same as (a1)-(a4), but according to honeycomb lattice. The scale dimension of all panels is 100×100.

3.1. Conical Diffraction

The propagation of a Gaussian beam $\psi_0 = \exp(-r^2/25)$ according to FSE is presented in Figs. 2(a1)-2(a4). Since the dispersion relation is linear, the light undergoes conical diffraction, as reported previously.[5] As a comparison, we also display the intensity distributions according to the DWE (5) and to the honeycomb lattice (6) propagation, in Figs. 2(b1)-2(b4) and Figs. 2(c1)-2(c4), respectively. We should note that we only excite the component ψ_+ by a Gaussian beam $\psi_0 = \exp(-r^2/25)$, and in Figs. 2(b1)-2(b4) only the component ψ_+ is shown. To excite the mode of the Dirac cone of the honeycomb lattice and obtain the conical diffraction in Figs. 2(c1)-2(c4), we launch the three beam interference pattern multiplied by a wide Gaussian beam $\psi_0 = \exp(-r^2/400)$ into one site of the honeycomb lattice,[20] since there are two sites in one unit cell. As expected, the conical diffraction is observed in all three cases. The appearance of wider and less resolved rings in Figs. 2(c1)-2(c4) is caused by the use of a wider Gaussian beam. Still, similar behavior is observed.

It is interesting to point out that the spreading speeds of the three conical diffractions in Fig. 2 are almost the same. For the first two cases, one can find that the relation between the radius of the ring r and the propagation distance z is $r/z = 1$, if one performs the Fourier transform of Eqs. (1) and (5). In the third case, the spreading speed is different in the continuum and discrete models; in the continuum model, the spreading speed is controlled by the potential coefficient V_0 (which here equals 1). It is worth mentioning that the Dirac cone still exists in shallow honeycomb lattices,[22] so the DWE is still valid.

Therefore, according to numerical simulations, the connection between the propagation dynamics in FSE and in honeycomb model indeed exists — it is the DWE. In other words, the honeycomb lattice represents potentially a real physical system that can be described by the FSE. Thus far, such real physical systems have been absent from the literature. The observable difference between the two in Fig. 2 is the presence of Poggendorff's dark ring[30] in the conical diffraction of the honeycomb lattice. The

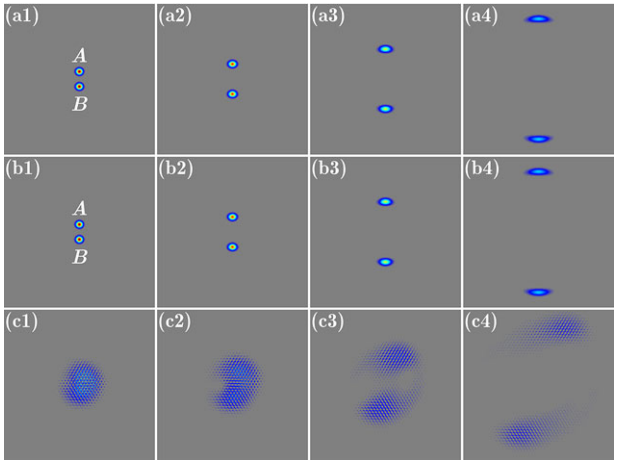

Figure 3. Same as Fig. 2, but for obliquely incident light beams.

reason is that there are two cones with opposite chiralities at the Dirac point of the honeycomb lattice, whereas there is only one cone in the FSE (as shown in Fig. 4 below).

3.2. Oblique Incidence

To further demonstrate the similarity between evolution described by the FSE and evolution in the honeycomb lattice, we investigate the propagation of obliquely incident beams according to FSE, DWE, and the honeycomb lattice. This is shown in **Figure 3**, which is set similarly to Fig. 2.

In Figs. 3(a1)-3(a4), the propagation of two obliquely incident Gaussian beams $\psi_{1,0} = \exp(-r^2/25)\exp(i2y)$ and $\psi_{2,0} = \exp(-r^2/25)\exp(-i2y)$ according to the FSE is depicted. As stated by the rule defined previously,[5] the beam centers will be at $(x, y) = z(0, \pm 1)$ during propagation; that is, the two beams in propagation will separate linearly from each other in the plane $x = 0$, as presented in Figs. 3(a1)-3(a4). Different from the FSE case, in the DWE case in Figs. 3(b1)-3(b4), the propagation of only one obliquely incident Gaussian beam $\psi_0 = \exp(-r^2/25)\exp(i2y)$ is displayed. One finds that the obliquely incident Gaussian beam splits into two Gaussian beams during propagation, and the behavior of these two Gaussian beams is the same as the behavior in Figs. 3(a1)-3(a4). For comparison, the propagation of a slightly oblique beam that excites the Bloch mode of the Dirac cone is exhibited in Figs. 3(c1)-3(c4). One must remember that the dispersion can only be viewed as linear in a small region around the Dirac point, and this is the reason why we choose a slightly oblique beam with a wide width.

The explanation of the propagation behavior observed in Fig. 3 is quite direct. As displayed in **Figure 4**, we inspect the momentum spectra corresponding to the evolution described by FSE, DWE, and the Schrödinger equation in the honeycomb lattice. In Fig. 4(a), the input two Gaussian beams will excite the Bloch modes located at sites A and B, respectively. Whereas in Fig. 4(b), only one input Gaussian beam can excite two Bloch modes at sites A and B, because the Bloch modes are degenerate only at the Dirac point, and the degeneracy is lifted if there is a shift in the momentum space. Since the dispersion along the polar direction is linear, as represented by the red lines in Figs. 4(a) and 4(b), the beam width along the vertical direction in Figs. 3(a) and 3(b) does not change. However, along the angular direction, as indicated by the red ellipses in Figs. 4(a) and 4(b), the dispersion is quadratic, which means the beams will spread along the horizontal direction, as shown in Figs. 3(a) and 3(b).

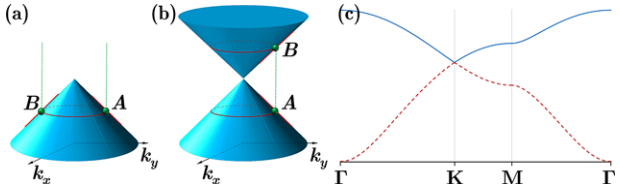

Figure 4. Momentum spectra of (a) FSE, (b) DWE, and (c) honeycomb lattice in the first Brillouin zone along high symmetric points.

One has reasons to believe that the two beams will evolve into a structure that is close to the conical diffraction with the increasing propagation distance, and the smaller the obliquity angle, the smaller the propagation distance to observe the conical-diffraction-like structure. This is more readily observed in Fig. 4(c) than in Figs. 4(a) or 4(b). In that figure, corresponding to Fig. 1(c), the band structure is shown along high-symmetry points. The Dirac point is at **K**, and one cannot excite the Bloch mode far away from **K**, to guarantee the linear dispersion. Therefore, one has to prepare the input beam that meets two conditions: large width and small slope. In Fig. 3(c), the input beam is the three-wave interference pattern which is multiplied by a wide Gaussian beam $\exp(-r^2/400)\exp(iy/10)$. Since there are more than two bands in this continuum model, the wide input may excite additional Bloch modes belonging to other bands, which will cause the movement of wide split beams in the circular direction – as seen in Fig. 3(c). Nevertheless, one still may agree that the phenomena observed in FSE can also be obtained in the honeycomb lattice. In other words, the honeycomb lattice can well mimic the behavior in FSE.

4. Conclusion

In conclusion, we have investigated the similarities between evolution described by the FSE and evolution in the honeycomb lattice described by the usual Schrödinger equation. We have found that the connection between the two can be established via the DWE. Numerical simulations support our theoretical predictions. However, such a link is not generally feasible, because when an additional potential is considered, the translational symmetry of the honeycomb lattice is broken,[13] which leads to the disappearance of Dirac cones. We believe that our work is a significant attempt to find a real physical system that can be described by the FSE, which may inspire new ideas on how to build novel and dispersion-controllable optical systems.

Appendix

The solution of Eq. (6) can be written as $\phi_n(\hat{r}, \hat{k})\exp(i\beta_n\hat{k}z)$, in which $\phi_n(\hat{r}, \hat{k})$ is the Bloch mode and $\beta_n(\hat{k})$ is the corresponding

propagation constant. Plugging this solution into Eq. (6), one obtains

$$-\beta_n\phi_n + \nabla^2\phi_n + V_h(x, y)\phi_n = 0, \tag{A1}$$

which is the standard eigenvalue problem. The Bloch mode ϕ_n is periodic with respect to $\hat{k}$, so it can be expanded in the Fourier series:

$$\phi\left(\hat{r}, \hat{k}\right) = \sum_{m,n} w_{m,n}\left(\hat{r}\right) \exp\left(-im\hat{k}\cdot\hat{v}_1 - in\hat{k}\cdot\hat{v}_2\right), \tag{A2}$$

where $w_{m,n}(\hat{r}) = \frac{1}{\Omega'}\int_{\Omega'}\phi(\hat{r}, \hat{k})\exp(-im\hat{k}\cdot\hat{v}_1 - in\hat{k}\cdot\hat{v}_2)d\hat{k}$ is so-called Wannier function. Here Ω' is the Brillouin zone. From the definition, one has that $w_{m,n}(\hat{r}) = w_{0,0}(\hat{r} - \hat{R}_{m,n})$ where $\hat{R}_{m,n} = m\hat{v}_1 + n\hat{v}_2$ denotes the position of the cell with indices (m, n).

Since $\beta_n(\hat{k})$ is also periodic, it can also be expanded in the Fourier series,

$$\beta(\hat{k}) = \sum_{m,n}\beta_{m,n}\exp\left(-im\hat{k}\cdot\hat{v}_1 - in\hat{k}\cdot\hat{v}_2\right). \tag{A3}$$

Due to the properties of Wannier function, the solution of Eq. (6) can be written as

$$\psi(\hat{r}, z) = \sum_{m,n,\alpha} C_{m,n,\alpha}(z)w_\alpha\left(\hat{r} - \hat{R}_{m,n}\right)\exp\left(-i\hat{k}\cdot\hat{R}_{m,n}\right), \tag{A4}$$

with α being the index of different bands.

In the tight-binding approximation, the honeycomb lattice can be broken into two triangular sublattices: A and B lattices. Close to the Dirac point, and due to the degeneracy, Eq. (A4) can be recast into

$$\psi(\hat{r}, z) = \sum_{m,n} a_{m,n}(z)w\left(\hat{r} - \hat{A}_{m,n}\right)\exp\left(-i\hat{k}\cdot\hat{A}_{m,n}\right) + \sum_{m,n} b_{m,n}(z)w\left(\hat{r} - \hat{B}_{m,n}\right)\exp\left(-i\hat{k}\cdot\hat{B}_{m,n}\right). \tag{A5}$$

Substituting Eqs. (A3) and (A5) into Eq. (6), one gets

$$\sum_{m,n} i\frac{da_{m,n}}{dz}S_A(m, n) - \sum_{m',n'}\beta_{m',n'}a_{m-m',n-n'}S_A(m - m', n - n')\exp\left(-i\hat{k}\cdot\hat{R}_{m',n'}\right) + i\frac{db_{m,n}}{dz}S_B(m, n) - \sum_{m',n'}\beta_{m',n'}\cdot b_{m-m',n-n'}S_B(m - m', n - n')\exp\left(-i\hat{k}\cdot\hat{R}_{m',n'}\right) = 0. \tag{A6}$$

Here, we introduce the notation $S_A(m, n) = w(\hat{r} - \hat{A}_{m,n})\exp(-i\hat{k}\cdot\hat{A}_{m,n})$ and $S_B(m, n) = w(\hat{r} - \hat{B}_{m,n})\exp(-i\hat{k}\cdot\hat{B}_{m,n})$.

Assuming $|\beta_{00}| \gg \left|\beta_{m,n}\right|$ with $m \neq 0$ and $n \neq 0$, multiplying Eq. (A6) by $S_A^*(\bar{m}, \bar{n})$ (the bar is dropped below), integrating over the whole $\hat{r}$ space, introducing the quantity

$$\epsilon = \frac{\int\tilde{w}^*\left(\hat{r} - \hat{A}_{m,n}\right)\tilde{w}\left(\hat{r} - \hat{B}_{m,n}\right)d\hat{r}}{\int\left|\tilde{w}(\hat{r} - \hat{A}_{m,n})\right|^2 d\hat{r}}, \tag{A7}$$

and keeping the dominant terms, one ends up with

$$i\frac{da_{m,n}}{dz} - \beta_{0,0}a_{m,n} - \epsilon\beta_{0,0}\left[b_{m-1,n}\exp\left(i\hat{k}\cdot\hat{d}_3\right) + b_{m,n-1}\exp\left(i\hat{k}\cdot\hat{d}_2\right) + b_{m,n}\exp\left(i\hat{k}\cdot\hat{d}_1\right)\right] = 0. \tag{A8}$$

Notice that $w(\hat{r} - \hat{A}_{m,n})$ is localized around $\hat{A}_{m,n}$ and independent of (m, n). Also note that $|\beta_{00}| \gg \left|\beta_{m,n}\right|$ is only valid for deep potentials. For our case in Eq. (7), the condition is not satisfied strictly, but it still can serve as a non-shallow potential. In a similar fashion, the other equation is obtained

$$i\frac{db_{m,n}}{dz} - \beta_{0,0}b_{m+1,n} - \epsilon\beta_{0,0}\left[a_{m+1,n}\exp\left(-i\hat{k}\cdot\hat{d}_3\right) + a_{m,n+1}\exp\left(-i\hat{k}\cdot\hat{d}_2\right) + a_{m,n}\exp\left(-i\hat{k}\cdot\hat{d}_1\right)\right] = 0, \tag{A9}$$

where $\hat{d}_1 = \hat{A}_{m,n} - \hat{B}_{m,n} = l(0, -1)$, $\hat{d}_2 = \hat{A}_{m,n} - \hat{B}_{m,n-1} = l(-\sqrt{3}/2, 1/2)$ and $\hat{d}_2 = \hat{A}_{m,n} - \hat{B}_{m-1,n} = l(\sqrt{3}/2, 1/2)$.

We focus on the propagation of a light beam with wave number $\hat{k}$ in the vicinity of Dirac point $\mathbf{K} = (\frac{4\pi}{3\sqrt{3}l}, 0)$. From equations above, one gets the discrete equations

$$i\frac{da_{m,n}}{dz} - \beta_{0,0}a_{m,n} - \epsilon\beta_{0,0}\left[b_{m-1,n}\left(-\frac{1}{2} + \frac{\sqrt{3}i}{2}\right) + b_{m,n-1}\left(-\frac{1}{2} - \frac{\sqrt{3}i}{2}\right) + b_{m,n}\right] = 0, \tag{A10}$$

and

$$i\frac{db_{m,n}}{dz} - \beta_{0,0}a_{m,n} - \epsilon\beta_{0,0}\left[a_{m+1,n}\left(-\frac{1}{2} - \frac{\sqrt{3}i}{2}\right) + a_{m,n+1}\left(-\frac{1}{2} + \frac{\sqrt{3}i}{2}\right) + a_{m,n}\right] = 0. \tag{A11}$$

Taking the continuum limit approximation, after some algebra, one obtains the governing equations for a and b:

$$\frac{da}{dz} - \beta_{0,0}a - \frac{\sqrt{3}}{2}\epsilon\beta_{0,0}\left(\partial_x b - i\partial_y b\right) = 0, \tag{A12}$$

and

$$i\frac{db}{dz} - \beta_{0,0}b + \frac{\sqrt{3}}{2}\epsilon\beta_{0,0}\left(\partial_x a + i\partial_y a\right) = 0. \tag{A13}$$

Notice that $\beta_{0,0}a$ and $\beta_{0,0}b$ can be absorbed into the first terms by defining new variables $\tilde{a} = a\exp(-i\beta_{0,0}z)$ and $\tilde{b} = b\exp(-i\beta_{0,0}z)$. So, one finally gets the Dirac equations for a and b:

$$i\frac{da}{dz} - D\left(-\partial_x + i\partial_y\right)b = 0, \tag{A14}$$

$$i\frac{db}{dz} - D\left(\partial_x + i\partial_y\right)a = 0. \tag{A15}$$

with $D = -\sqrt{3}\epsilon\beta_{0,0}/2$.

Acknowledgment

This work was supported by Natural Science Foundation of Shaanxi Province (2017JZ019, 2017JQ6039), China Postdoctoral Science Foundation (2016M600777, 2017T100734, 2016M600776), National Natural Science Foundation of China (11474228, 61605154), and Qatar National Research Fund (NPRP 8-028-1-001).

Conflict of Interest

The authors delcare no conflict of interest.

Keywords

Fractional Schrödinger equation, Honeycomb lattice, Linear dispersion, Dirac-Weyl equation

Received: April 21, 2017
Revised: May 22, 2017
Published online: July 13, 2017

[1] N. Laskin *Phys. Lett. A* **268**, 298–305 (2000).
[2] N. Laskin *Phys. Rev. E* **62**(Sep), 3135–3145 (2000).
[3] N. Laskin *Phys. Rev. E* **66**(Nov), 056108 (2002).
[4] Y. Q. Zhang, X. Liu, M. R. Belić, W. P. Zhong, Y. P. Zhang, and M. Xiao *Phys. Rev. Lett.* **115**(Oct), 180403 (2015).
[5] Y. Q. Zhang, H. Zhong, M. R. Belić, N. Ahmed, Y. P. Zhang, and M. Xiao *Sci. Rep.* **6**, 23645 (2016).
[6] Y. Q. Zhang, H. Zhong, M. R. Belić, Y. Zhu, W. P. Zhong, Y. P. Zhang, D. N. Christodoulides, and M. Xiao *Laser Photon. Rev.* **10**, 526–531 (2016).
[7] A. Liemert and A. Kienle *Mathematics* **4**(2), 31 (2016).
[8] B. Guo and D. Huang *J. Math. Phys.* **53**(8), 083702 (2012).
[9] C. Klein, C. Sparber, and P. Markowich *Proc. R. Soc. A* **470**(2172), 20140364 (2014).
[10] L. Zhang, C. Li, H. Zhong, C. Xu, D. Lei, Y. Li, and D. Fan *Opt. Express* **24**(13), 14406–14418 (2016).
[11] C. Huang and L. Dong *Opt. Lett.* **41**(24), 5636–5639 (2016).
[12] S. Longhi *Opt. Lett.* **40**(6), 1117–1120 (2015).
[13] L. Lu, J. D. Joannopoulos, and M. Soljačić *Nat. Photon.* **8**(11), 821–829 (2014).
[14] M. C. Rechtsman, J. M. Zeuner, Y. Plotnik, Y. Lumer, D. Podolsky, F. Dreisow, S. Nolte, M. Segev, and A. Szameit *Nature* **496**, 196–200 (2013).
[15] Y. Plotnik, M. C. Rechtsman, D. Song, M. Heinrich, J. M. Zeuner, S. Nolte, Y. Lumer, N. Malkova, J. Xu, A. Szameit, Z. Chen, and M. Segev *Nat. Mater.* **13**, 57–62 (2014).
[16] A. H. Castro Neto, F. Guinea, N. M. R. Peres, K. S. Novoselov, and A. K. Geim *Rev. Mod. Phys.* **81**(Jan), 109–162 (2009).
[17] H. Zhong, Y. Q. Zhang, Y. Zhu, D. Zhang, C. B. Li, Y. P. Zhang, F. L. Li, M. R. Belić, and M. Xiao *Ann. Phys. (Berlin)* **529**(3), 1600258 (2017), 1600258.
[18] M. J. Ablowitz, S. D. Nixon, and Y. Zhu *Phys. Rev. A* **79**(May), 053830 (2009).
[19] M. J. Ablowitz and Y. Zhu *Phys. Rev. A* **82**(Jul), 013840 (2010).
[20] D. Song, V. Paltoglou, S. Liu, Y. Zhu, D. Gallardo, L. Tang, J. Xu, M. Ablowitz, N. K. Efremidis, and Z. Chen *Nat. Commun.* **6**, 6272 (2015).
[21] D. Song, S. Liu, V. Paltoglou, D. Gallardo, L. Tang, J. Zhao, J. Xu, N. K. Efremidis, and Z. Chen *2D Mater.* **2**, 034007 (2015).
[22] M. J. Ablowitz and Y. Zhu *SIAM J. Appl. Math.* **72**, 240–260 (2012).
[23] M. Boguslawski, P. Rose, and C. Denz *Phys. Rev. A* **84**(Jul), 013832 (2011).
[24] G. Bartal, O. Cohen, H. Buljan, J. W. Fleischer, O. Manela, and M. Segev *Phys. Rev. Lett.* **94**(Apr), 163902 (2005).
[25] B. Freedman, G. Bartal, M. Segev, R. Lifshitz, D. N. Christodoulides, and J. W. Fleischer *Nature* **440**(7088), 1166–1169 (2006).
[26] S. Liu, P. Zhang, X. Gan, F. Xiao, and J. Zhao *Appl. Phys. B* **99**, 727–731 (2010).
[27] P. Zhang, S. Liu, C. Lou, F. Xiao, X. Wang, J. Zhao, J. Xu, and Z. Chen *Phys. Rev. A* **81**(Apr), 041801 (2010).
[28] O. Peleg, G. Bartal, B. Freedman, O. Manela, M. Segev, and D. N. Christodoulides *Phys. Rev. Lett.* **98**(Mar), 103901 (2007).
[29] Y. Q. Zhang, Z. K. Wu, M. R. Belić, H. B. Zheng, Z. G. Wang, M. Xiao, and Y. P. Zhang *Laser Photon. Rev.* **9**, 331–338 (2015).
[30] M. Berry and M. Jeffrey *Prog. Opt.* **50**, 13–50 (2007).